The Journal of Chemical Physics

RESEARCH ARTICLE | FEBRUARY 27 2024

Electro-osmotic flow in nanoconfinement: Solid-state and protein nanopores

Special Collection: Polymer Nanoconfinement

Minglun Li ; Murugappan Muthukumar

J. Chem. Phys. 160, 084905 (2024)
https://doi.org/10.1063/5.0185574

AIP Publishing

The Journal of Chemical Physics ARTICLE pubs.aip.org/aip/jcp

Electro-osmotic flow in nanoconfinement: Solid-state and protein nanopores

Cite as: J. Chem. Phys. 160, 084905 (2024); doi: 10.1063/5.0185574
Submitted: 31 October 2023 • Accepted: 5 January 2024 •
Published Online: 27 February 2024

Minglun Li and Murugappan Muthukumar[a)]

AFFILIATIONS

Department of Polymer Science and Engineering, University of Massachusetts, Amherst, Massachusetts 01003, USA

Note: This paper is part of the JCP Special Topic on Polymer Nanoconfinement.
[a)]**Author to whom correspondence should be addressed:** muthu2346@gmail.edu

ABSTRACT

Electro-osmotic flow (EOF) is a phenomenon where fluid motion occurs in porous materials or micro/nano-channels when an external electric field is applied. In the particular example of single-molecule electrophoresis using single nanopores, the role of EOF on the translocation velocity of the analyte molecule through the nanopore is not fully understood. The complexity arises from a combination of effects from hydrodynamics in restricted environments, electrostatics emanating from charge decorations and geometry of the pores. We address this fundamental issue using the Poisson–Nernst–Planck and Navier–Stokes (PNP–NS) equations for cylindrical solid-state nanopores and three representative protein nanopores (α-hemolysin, MspA, and CsgG). We present the velocity profiles inside the nanopores as a function of charge decoration and geometry of the pore and applied electric field. We report several unexpected results: (a) The apparent charges of the protein nanopores are different from their net charge and the surface charge of the whole protein geometry, and the net charge of inner surface is consistent with the apparent charge. (b) The fluid velocity depends non-monotonically on voltage. The three protein nanopores exhibit unique EOF and velocity–voltage relations, which cannot be simply deduced from their net charge. Furthermore, effective point mutations can significantly change both the direction and the magnitude of EOF. The present computational analysis offers an opportunity to further understand the origins of the speed of transport of charged macromolecules in restricted space and to design desirable nanopores for tuning the speed of macromolecules through nanopores.

I. INTRODUCTION

Movement of charged macromolecules under confinement in the presence of externally applied electric fields is an extremely important phenomenon in the general context of single-molecule direct sequencing of biological polymers using electrophoresis through nanopores as well as in many biologically relevant situations.[1–4] In the technique of single-molecule electrophoresis using a single nanopore, ionic current is measured and its modulations during the translocation of a particular molecule are used to characterize the molecule in terms of its chemical sequence, size, contour length, etc. Over the past several decades, considerable achievements have been made in designing the nanopores to improve sequencing accuracy, fabrication of solid-state nanopores,[5–7] and the synthetic/mutation of protein nanopores,[8] along with a significant molecular understanding of translocation of charged macromolecules through a nanopore.[9] In spite of these advances, the role of hydrodynamics in the ubiquitous phenomenon of movement of charged macromolecule under confinement is not yet adequately addressed.

The nanopore provides confined space as small as a few nanometers in radius, the inhomogeneous charge distribution, and the chemical group modification. When these factors are combined within the confinement system, nanofluidic systems inherently display nonuniform characteristics. Meanwhile, an electro-osmotic flow (EOF) arises when the electric field acts on such an inhomogeneous system.[10–13] The fundamental origin of EOF is the interaction between the electric field and the charged species present in the electric double layer, which forms a layer of net charge near a charged surface. The ions will move under the external electric field and they drag the surrounding fluid with them, resulting in flow. In recent years, numerous studies have emphasized the significant influence of EOF on translocation processes.[14,15] In light of this, comprehending the behavior of EOF within nanoconfinement is crucial for the design of nanopore sequencing devices aimed at improving accuracy.

Due to these considerations, there has been a growing focus on nanofluids in the confinement.[16] A lot of studies have been made to reveal the effect of geometry and charge on EOF. For example, earlier experimental studies provided the first direct measurements of the force from EOF acting on DNA molecules during translocation through a solid-state nanopore.[14,17] Currently, researchers are capable of devising electro-osmotic traps to investigate the kinetic characteristics of biomacromolecules based on the aforementioned principles.[18] To promote the capture and analysis of folded proteins, it is even possible to create EOF by engineering the surface charge of protein nanopores.[19] Analytical methods precisely predicted the size of the capturing region[20,21] and translocation time as a function of salt concentration in bulk solution when the polymer translocated through a cylindrical nanopore.[22] Of the existing techniques, all-atom molecular dynamics (MD) simulations are the most directly capable of tracing water molecules in EOF.[23] Studies from Aksimentiev's group have shown that EOF produced by the high negative charge of the DNA channel's walls governs the transport of charged solutes, which can significantly improve translocation efficiency.[24] Results from Chinappi's group show that changes in solution pH significantly affect ionic and electro-osmotic flows through the α-hemolysin nanopore,[25] and lower pH gives rise to an intense EOF.

Due to the protein's soft surface, thousands of amino acids with charges, and an irregular shape,[26–28] studies on EOF in protein nanopores are still challenging. The principal obstacle lies in the difficulty of experimentally detecting EOF within protein nanopores.[29] Additionally, performing all-atom simulations for extensive systems remains a time-consuming undertaking, even with the availability of several accelerators.[30] The numerical method based on the finite element method provides an effective approach to solving this problem, which can give precise solutions for handling complex and irregular boundaries.[31,32] Nevertheless, despite these significant efforts to grasp the influence of EOF on translocation, a comprehensive understanding of EOF remains elusive. For example, considering the complexity of the protein nanopore, whether the classical EOF models (like cylindrical nanopores) can be applicable is unknown. There is a lack of systematic work that compares these models within the context of protein nanopores. Furthermore, it is crucial to investigate the differences in EOF behavior among typical protein nanopores.

The focus of the present paper is to compute EOF for several protein nanopores in the context of single-molecule electrophoresis. We have performed a series of numerical studies based on Poisson–Nernst–Planck and Navier–Stokes (PNP–NS) equations. By starting from the solid-state nanopore with cylindrical geometry to examine EOF properties, our investigations encompass the influences of surface charge and radius of the nanopore, the applied voltage between the *trans* and *cis* sides, and salt concentration in the bulk solution. Furthermore, we conduct a systematic comparison of EOF in three typical protein nanopores: α-hemolysin (α-HL),[26] Mycobacterium smegmatis porin A (MspA),[27] and curli transport lipoprotein (CsgG).[28] We provide detailed depictions of EOF flow velocity distributions in the protein nanopores (wild-type), which reveal a significantly nonhomogeneous distribution. Through our comparative study, we observe that both nanopores α-HL and MspA apparently exhibit negatively charged nanopores. While CsgG behaves more like a positively charged nanopore. These "apparent charge" properties are consistent with the net charges of inner surfaces of the protein nanopore. We discuss the influence of mutations on EOF by taking MspA as an example. We show that some effective point mutations can significantly change both the direction and the magnitude of EOF. These findings hold significant implications, serving as valuable reference points and guiding principles for the future design of novel nanopore systems.

II. METHOD

A. Theoretical expressions

The nanopore system includes the charged nanopore, electrolyte solution with free ions and water molecules, and the external electric field between the *trans* and *cis* sides. In order to get the velocity distribution, our complete system is described by a series of coupled partial differential equations: Poisson–Nernst–Planck equations for the electrostatic field and ion distributions[33–36] and the Navier–Stokes equation for fluid flow.[9]

The electrostatic potential (Φ) of the nanopore is a combination of the applied potential, charges in the nanopore, and ions in the solution, which it is done by self-consistently solving the Poisson equation:

$$\nabla \cdot [\varepsilon_0 \varepsilon(\mathbf{r}) \nabla \Phi(\mathbf{r})] = -[\rho_{\text{pore}}(\mathbf{r}) + \rho_{\text{ion}}(\mathbf{r})]. \tag{1}$$

Here, the vector $\mathbf{r}$ refers to any spatial position in the system. ε_0 is the vacuum permittivity (8.854×10^{12} F m^{-1}), ε is the relative permittivity, we use $\varepsilon = 78$ and 20, respectively, for water reservoir and protein nanopore.[31] $\rho_{\text{pore}}(\mathbf{r})$ is the charge density of the solid-state/protein nanopore, which (for protein pores) was calculated from the all-atom Protein Data Bank (PDB) coordinates by Eq. (9) given below. The charge density of mobile ions in the system is given by

$$\rho_{\text{ion}}(\mathbf{r}) = e c_{\text{net}}(\mathbf{r}) = e \sum_i z_i c_i(\mathbf{r}), \tag{2}$$

where e, z_i, and $c_i(\mathbf{r})$ are, respectively, the electronic charge, the valency of the ion, and the number density of the ion. $c_{\text{net}}(\mathbf{r})$ is the concentration of net charge.

The ionic flux of each i-th ion $\boldsymbol{J}_i(\mathbf{r})$ is expressed by the Nernst–Planck equation:

$$\boldsymbol{J}_i(\mathbf{r}) = -D_i \left[\nabla c_i(\mathbf{r}) + \frac{z_i c_i(\mathbf{r})}{k_{\text{B}} T} \nabla \Phi(\mathbf{r}) \right], \tag{3}$$

where D_i is the diffusion coefficient of ions. $k_{\text{B}}T$ is the Boltzmann constant times desired temperature. In our calculation, $D_{\text{K+}} = 1.96 \times 10^{-9}$ m^2/s and $D_{\text{Cl-}} = 2.032 \times 10^{-9}$ m^2/s.[31,37] For the steady state, we have

$$\frac{\partial c_i(\mathbf{r}, t)}{\partial t} = -\nabla \cdot \boldsymbol{J}_i(\mathbf{r}) = 0. \tag{4}$$

The time dependence of the velocity of fluid flow ($\boldsymbol{v}$) is obtained by the Navier–Stokes equation:

$$\omega_0 \frac{\partial \boldsymbol{v}(\mathbf{r}, t)}{\partial t} + \boldsymbol{v} \cdot \nabla \boldsymbol{v}(\mathbf{r}, t) - \eta \nabla^2 \boldsymbol{v}(\mathbf{r}, t) + \nabla p(\mathbf{r}, t) = \boldsymbol{F}(\mathbf{r}, t), \tag{5}$$

where $p(\mathbf{r}, t)$ is the local pressure field, ω_0 is the mass density of the fluid, and η is the shear viscosity of the fluid, we use $\eta = 8.904 \times 10^{-4}$ Pa · s for water.[31] $\boldsymbol{F}(\mathbf{r}, t)$ is an external force.

As the practical system lies in the weak velocity fields and considers the steady state condition, the first two terms on the left-hand side of the above equation may be ignored to give[38]

$$-\eta\nabla^2\boldsymbol{v}(\mathbf{r}) + \nabla p(\mathbf{r}) = \boldsymbol{F}(\mathbf{r}). \tag{6}$$

Based on the assumption that the fluid is incompressible $\nabla\cdot\boldsymbol{v}(\mathbf{r}) = 0$ and thus the pressure field in Eq. (6) can be eliminated, we get the Navier–Stokes equation for the creeping flow:

$$-\eta\nabla^2\boldsymbol{v}(\mathbf{r}) = \rho_{\text{ion}}(\mathbf{r})\boldsymbol{E}(\mathbf{r}), \tag{7}$$

where $\rho_{\text{ion}}(\mathbf{r})\boldsymbol{E}(\mathbf{r}) = \boldsymbol{F}(\mathbf{r})$. $\boldsymbol{E}(\mathbf{r})$ is the electric field of the nanopore working on the ions at position $\mathbf{r}$ (inside the nanopore), and the electric field is the gradient of the electric potential $\boldsymbol{E}(\mathbf{r}) = -\nabla\Phi(\mathbf{r})$.

B. Geometry and charge distribution of the model

The above partial differential equations are solved by finite element solver COMSOL Multiphysics (v5.4, COMSOL Inc., Burlington, MA, USA), and the basic calculation framework follows the method from the work of Willems *et al.*[31] Both the solid-state and protein nanopores have a high degree of radial symmetry structures. Setting up the whole system as a 2D-axisymmetric model can significantly save computing time.[39] The whole system is schematically shown in Fig. 1(a). It consists of a hemispherical electrolyte reservoir with a radius (R) of 200 nm. A flat wall (corresponding to the membrane carrying the nanopore) that separates the *cis* and *trans* chambers is placed in the middle. The nanopore is then placed at the center. The thickness of this wall is 10 nm for solid-state nanopores and 2.74 nm for the lipid bilayer in protein nanopore assemblies. The thickness of the lipid bilayer we used is estimated from the all-atomic coordinates of the phosphatidylcholine lipids, where the coordinates (DDPC) are provided by CHARMM-GUI.[40] This number is also consistent with the calculation from the input (2.8 nm) presented in the work of Willems *et al.*[31] The lipid bilayer we considered in this work is charge neutral and long enough so that its thickness has little effect on the results of the calculations.

In order to realize 2D-axisymmetric calculations, we need to make the reduction of the three-dimensional geometry and charge distribution to two dimensions. For the cylindrical nanopore, the geometry has already been constructed by the flat region with a nanopore in the center. Uniformly distributed charges have been assigned to the columnar surface (the blue line in the first column of Fig. 1(b)). For the protein nanopores, we get the geometry through the atomic density map [Eq. (8)] and charge density in a pseudo-3D space through the atomic partial charges [Eq. (9)].

We computed the three-dimensional atomic density maps from the all-atom coordinates of the protein nanopores, which the structures were from Protein Data Bank (PDB)[41] with the entry IDs are 7AHL, 1UUN, and 4UV3 respectively for α-HL, MspA, and CsgG. We used PBD2PQR[42] and the web server[43] to add the missing hydrogen atoms and used PROPKA[44,45] method to assign

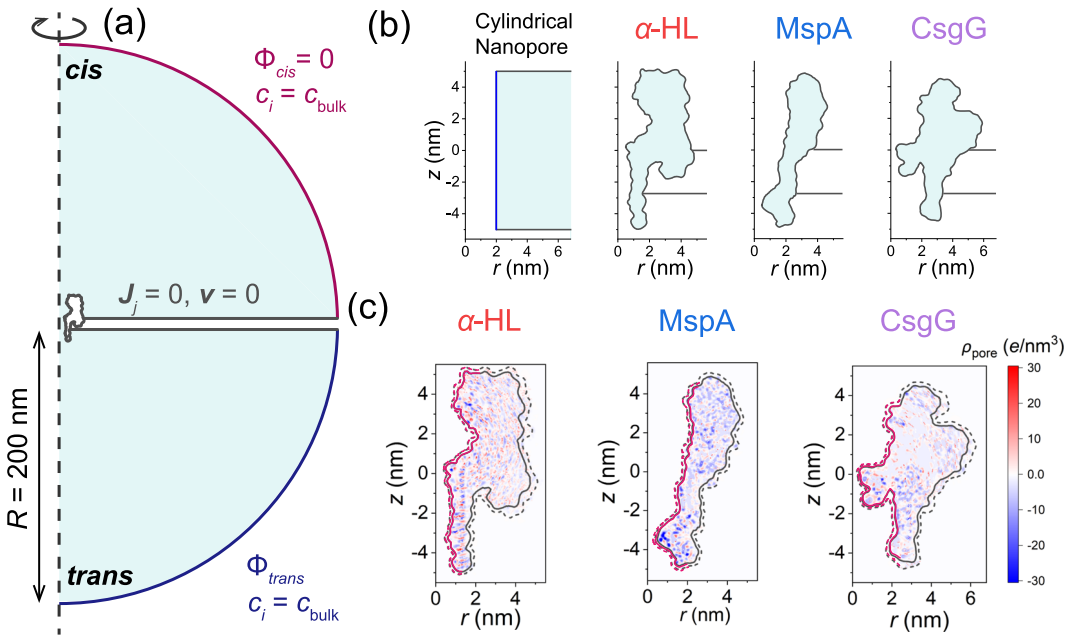

FIG. 1. (a) Representative schematic of the calculation system: the 2D-axisymmetric geometry of α-HL assembled with either a solid layer or a lipid bilayer and surrounded by a spherical water reservoir (light green). (b) The 2D-axisymmetric geometries studied in this work, and the boundaries of protein nanopores denote the contour lines corresponding to 25% atomic density in their density maps (Fig. S1). (c) The charge density in three-dimensional space of the three protein nanopores, which is calculated by $\rho_{\text{pore}}(r,z)/2\pi r$. The detailed expression is given in Eq. (9). The short dash and solid lines are respectively the 4% and 25% protein atomic density. The inner-surface area is shown in red, and the criterion values of r and z are as follows: α-HL: $r \leqslant 1.36$ and $z \leqslant 0$, $r < 2.26$ and $z > 0$; MspA: $r \leqslant 2$ and $z \leqslant -2$, $r < 2.5$ and $z > -2$; CsgG: $r \leqslant 2.37$ nm.

protonation states at pH = 7. The mapping of the 2D density map from three-dimensional spaces is assigned to 0.5 Å resolution grid using the Gaussian function:[46]

$$\tilde{c}_{\text{pore}} = 1 - \prod_i \left[1 - \exp\left(-\frac{d_i^2}{(\sigma r_{\text{vdW},i})^2}\right)\right], \tag{8}$$

where $\tilde{c}_{\text{pore}}$ refers to the normalized number density of the atoms in the space, for which the reference value is 1 for each grid. For each atom i, $r_{\text{vdW},i}$ is the van der Waals radius, and $\sigma = 0.93$ is a width factor. $d_i = [(x - x_i)^2 + (y - y_i)^2 + (z - z_i)^2]^{1/2}$ is the distance of grid coordinates (x, y, z) from the target atom center (x_i, y_i, z_i). The resulting three-dimensional density map was then radially averaged along the z-axis, relative to the center of the nanopore to obtain a 2D-axisymmetric density map. The 2D-axisymmetric density map results (r-z axis) of the three nanopores are shown in Fig. S1, and the contour line at 25% density was used as the boundary of the nanopore geometry [Fig. 1(c) and S1].

The partial charges of nanopores at atomic level are also obtained by PBD2PQR,[42,43] and the force field is CHARMM.[47] We also check the output of PQR results by selecting other force field in the web server, like AMBER,[48] the partial charges are the same. Thus, the output of force field from the standard web server does not influence the results in this work. We should note that this is the output of the server. If we use other methods to get the partial charge in different force fields like "gmx pdb2gmx" in GROMACS, the partial charges of the force fields CHARMM and AMBER may differ. The charge distribution of the nanopore at specific points in two-dimensional space $\rho_{\text{pore}}(r, z)$ is calculated by[31,49]

$$\rho_{\text{pore}}(r, z) = \sum_i \frac{e\delta_i}{\pi\left(\sigma' r_{\text{vdW},i}\right)^2} \exp\left[-\frac{(r - r_i)^2 + (z - z_i)^2}{\left(\sigma' r_{\text{vdW},i}\right)^2}\right], \tag{9}$$

where δ_i is the partial charge in the three-dimensional space (x_i, y_i, z_i), which contributes $\delta_i/(2\pi r_i)$ in two-dimensional space $r_i = (x_i^2 + y_i^2)^{1/2}$. $\sigma' = 0.5$ is used for the calculation and the grid resolution is 0.1 Å. A Gaussian distribution of the space charge density of each atom i around its respective 2D-axisymmetric coordinates is considered in Eq. (9). The van der Waals radius and partial charge of each atom are obtained by PBD2PQR[42] by inputting the PDB file of each protein nanopore. The results of the charge density in the above calculation are the results of charge density in three-dimensional space mapping to two-dimensional space. Within COMSOL Multiphysics, the data of $\rho_{\text{pore}}(r, z)$ are imported as a 2D linear interpolation function and converted into a pseudo-3D volumetric charge density through $\rho_{\text{pore}}(r, z)/2\pi r$ as shown in Fig. 1(c).

C. Boundary conditions

The boundary conditions of the whole system are broadly divided into two classes: the boundary of the reservoir; the nanopore and the flat (lipid) membrane. The schematic is illustrated in Fig. 1(a). The potential of the *cis* side is grounded ($\Phi_{cis} = 0$) and a fixed bias potential Φ_{trans} was applied along the *trans* edge. The salt concentrations (monovalent cations and anions in this study) at these two boundaries are fixed as $c_+ = c_- = c_{\text{bulk}}$. The flow is enabled by the "no normal stress" condition. The surface of flat or lipid bilayer and edges of the nanopore are treated with no-flux ($\boldsymbol{J}_i = 0$) and no-slip ($\boldsymbol{v} = 0$) conditions, which means that ions and water molecules cannot pass through the membrane and that the fluid velocity $\boldsymbol{v}$ is zero.

D. Limitations

Even though a full three-dimensional model is preferable, which requires substantial computational demands, we use only 2D-axisymmetric approach. This is based on the assumption that both the geometry and charge distribution are almost radially symmetric. Although there are a few localized asymmetries for the three protein nanopores in this work, we expect that their consequences are only minor. Since the applied voltages in the experiments are small, we ignore the nonlinear terms in velocity in accounting for hydrodynamics. Furthermore, we have ignored the concentration dependencies of ion diffusion coefficients, electrophoretic mobilities, electrolyte viscosity, density, and relative permittivity.[31]

III. SOLID-STATE NANOPORES WITH CYLINDRICAL GEOMETRY

Solid-state nanopores are tiny holes, typically with a radius ranging from 1 to 10 nm, fabricated in thin insulating membranes. For the applications of translocation, the solid-state nanopore is robust and highly customizable, and the size, shape, and surface properties can be precisely controlled during fabrication. In most cases, the solid-state nanopore has cylindrical geometry as shown in Fig. 2(a).[50] The velocity of EOF within this cylindrical geometry is a classical problem with analytical solutions.[20] From Eq. (7), the velocity of EOF $\boldsymbol{v}(\mathbf{r})$ is directly determined by the net local charge concentration $\rho_{\text{ion}}(\mathbf{r})$ and electric field $\boldsymbol{E}(\mathbf{r})$. In this section, our primary focus lies on examining the determinants of $\rho_{\text{ion}}(\mathbf{r})$ and $\boldsymbol{E}(\mathbf{r})$, and consequently EOF. This includes the charge density of the nanopore's inner surface, applied voltage, ion concentration in the bulk solution, and the nanopore's radius. After establishing the validity of the present numerical scheme for this classical problem, we will compute EOF for the more complex protein nanopores.

We investigate the impact of charge density σ on the inner surface of the nanopore by assigning different charge densities (−0.624, 0, 0.062, 0.312, and 0.624 e/nm^2) while keeping other parameters constant. In our setup, the direction of the external electric field is from negative to positive along the z-axis direction. The velocity distributions in two dimensions for the positively and negatively charged nanopore are presented in Figs. 2(b) and 2(c), respectively. A positively charged nanopore causes EOF in the opposite direction to the electric field, while a negatively charged nanopore results in EOF in the same direction as the electric field. For cylindrical nanopores, the velocity of EOF $\boldsymbol{v}$ well inside the pore is essentially the same at a given radial position r, except near the entrance of the *trans* and *cis* sides. Taking the radial direction at $z = 0$ for example [Fig. 2(d)], the magnitude of $\boldsymbol{v}$ increases nonlinearly from the nanopore wall ($r = \pm 2$ nm) toward the center ($r = 0$ nm) and tends to plateau near the center. At any specific radial position r, $\boldsymbol{v}$ increases with surface charge density. This nonlinear velocity profile is due to the presence of an electrical double layer, which is caused by the attraction of counterions near the charged surface. The length scale

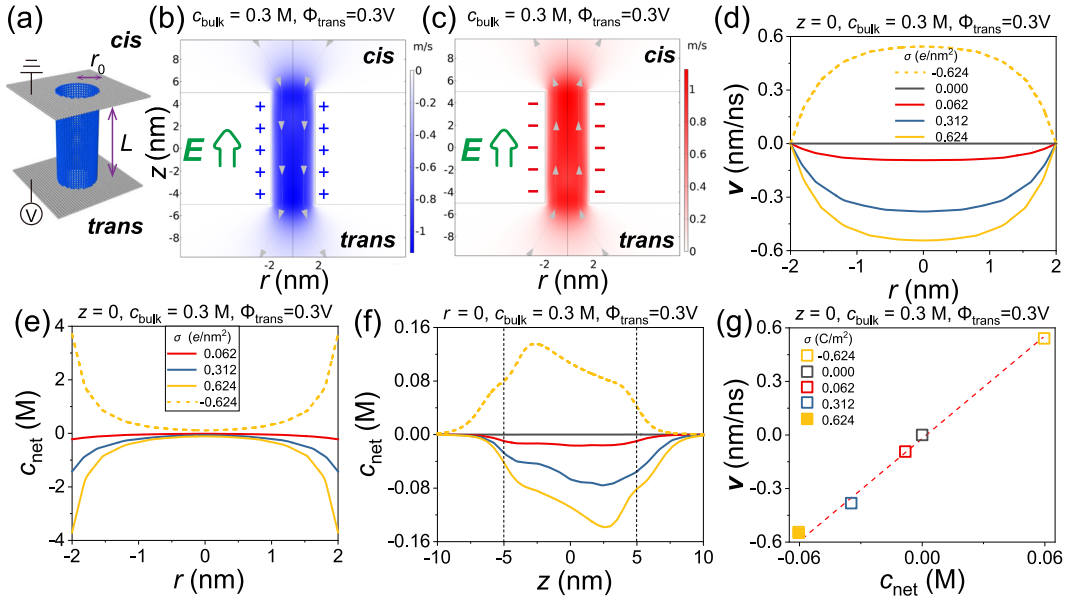

FIG. 2. (a) Schematic of solid-state nanopore with a cylindrical geometry, r_0 is the radius and L = 10 nm is the length of the nanopore. (b), (c) Velocities of EOF in r-z plane for positively (0.624 e/nm^2) and negatively (−0.624 e/nm^2) charged nanopores. (d) Velocity $\boldsymbol{v}$ of the radial direction at z = 0. (e), (f) Net charge concentration c_{net} along r-axis and z-axis, the legends are the same as shown in (e). (g) Velocity $\boldsymbol{v}$ as a function of net charge concentration c_{net}.

of this double layer can be estimated by the Debye length.[51] From the results of the cation/anion and net charge concentration $c_{net} = \rho_{ion}/e$ in Figs. 2(e) and 2(f), and Figs. S2(a) and S2(b), the higher charge density of the wall surface will attract more counterions, and leads to the higher values of c_{net}. The average electric field from the *trans* side to the *cis* side is the same for the given applied voltage, although there is a little difference locally at different z positions [Figs. S2(c) and S2(d)]. Therefore, EOF is highly affected by c_{net} in addition to the electric field according to Eq. (7). Furthermore, we find that the relationship between $\boldsymbol{v}$ and c_{net} is linear for a given applied voltage [Fig. 2(g)].

Translocation behavior is significantly influenced by the applied voltage, denoted as Φ_{trans}. Consequently, understanding the relationship between the velocity of EOF $\boldsymbol{v}$, and the applied voltage is imperative. In Fig. 3(a), we plot the radial velocity distribution of EOF at z = 0, with a surface charge density of 0.624 e/nm^2. In general, similar to our previous observations, $\boldsymbol{v}$ exhibits a nonlinear increase from the nanopore wall toward its center and ascends with an increase in Φ_{trans}. Notably, when Φ_{trans} equals 3.5 V, $\boldsymbol{v}$ initially grows nonlinearly but subsequently diminishes, which exhibits a "W" shape. This behavior is linked to the observation that the strength of the electric field escalates with an increase in applied voltage [Figs. S3(a) and S3(b)]. The non-monotonicity of $\boldsymbol{v}$ is caused by the net charge concentration c_{net} according to Eq. (7). The calculated results given in Figs. 3(b) and 3(c) and Figs. S3(c) and S3(d) show that as the applied voltage increases, c_{net} changes from negative to positive (wall to center) for Φ_{trans} = 3.5 V. This shift in c_{net}'s sign implies the emergence of localized velocities that oppose the primary solvent motion direction, leading to a reduced flow velocity.

A deeper analysis of computed results reveals that ion distribution within the nanopore predominantly results from the competition between the charge density of the nanopore and the longitudinal electric field [Figs. 3(d) and 3(e)]. In the case of a positively charged pore wall, for example, when the attracting force provided by the wall is greater than the force from the electric field [Fig. 3(d)], more anions accumulate near the interface.[52,53] As a result, the fluid velocity contribution arising from the interfacial charge dominates over the electrophoretic contribution at the central axis of the pore. On the other hand, if the electric field is too strong, c_{net} at the interior of the pore can change its sign, as shown in Figs. 3(b) and 3(c). This in turn creates a velocity opposing the velocity field generated by the charged interface. This is schematically shown in Fig. 3(e). It is essential to highlight that our study's voltage range aligns with experimental conditions. Therefore, scenarios involving much higher voltages that could induce turbulence are not addressed. Building on this foundation, the dependency of averaged $\bar{\boldsymbol{v}}$ on the averaged electric field $\bar{E}$ about various surface charge densities σ is plotted in Fig. 3(f). At lower σ (like σ = 0.062 and ±0.624 e/nm^2), the relationship between $\bar{\boldsymbol{v}}$ and $\bar{E}$ is nonlinear. For weak electric fields, $\bar{\boldsymbol{v}}$ is directly proportional to the applied electric field as expected. However, as the applied electric field becomes progressively stronger, at a given surface charge density, the above-mentioned local velocity reversal becomes significant, resulting in a retardation effect on the net EOF velocity. In fact, this retardation effect can become so strong at even higher electric fields that the nonlinear behavior can exhibit non-monotonicity. By further increasing the applied voltage, the direction of EOF becomes the same as the electric field direction, which in turn leads to increased localized flow

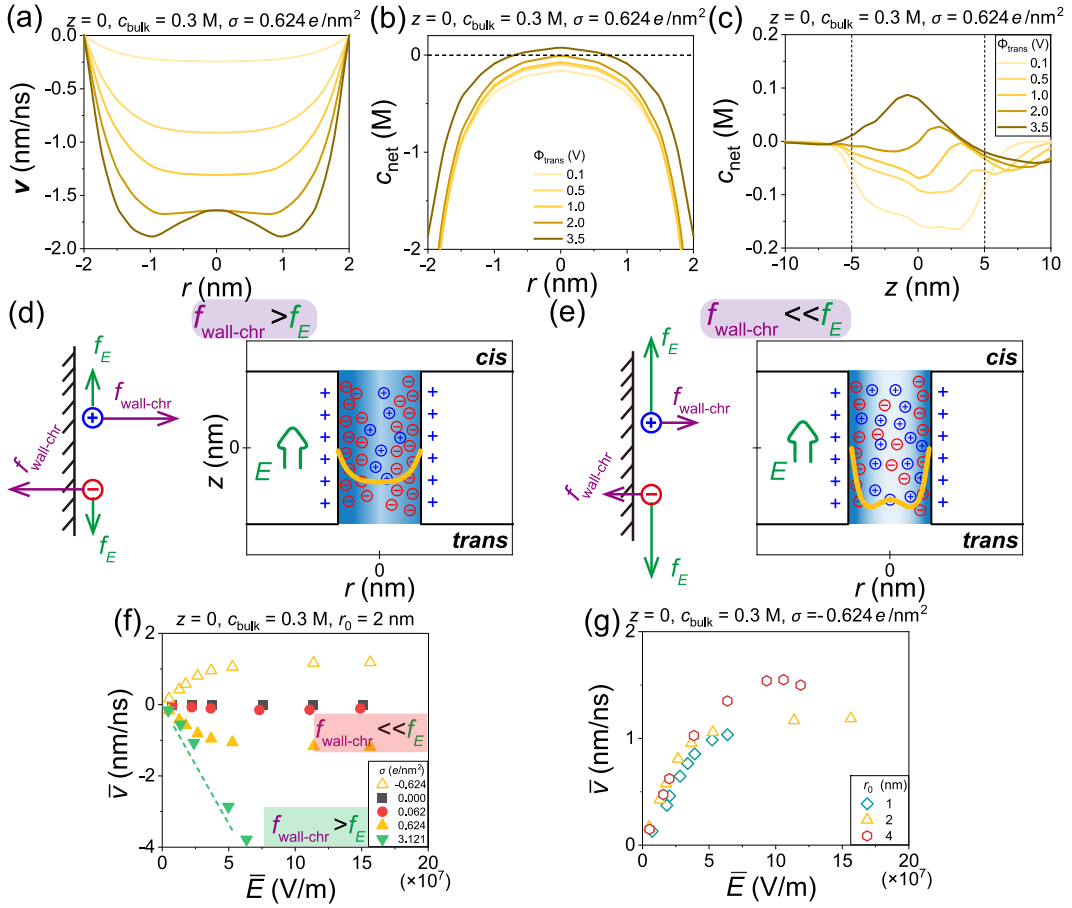

FIG. 3. (a) EOF velocity $\boldsymbol{v}$ in the radial direction at $z = 0$, the legend is the same as for (b) and (c). (b), (c) Net charge concentration c_{net} along r-axis and z-axis, the short dashed lines refer to the region of the solid-state nanopore. $c_{net} = c_{K+} - c_{Cl-}$, c_{K+} and c_{Cl-} are, respectively, the concentration of K^+ and Cl^-. Schematics of the electric forces acting on ions and distribution of ions in the nanopores with (d) lower and (e) higher applied voltages, where $f_{wall-chr}$ and f_E, respectively, refer to the forces of the charged wall of the nanopore and the electric field. Relationship between velocity $\bar{v}$ and electric field $\bar{E}$ averaged over the radial direction at $z = 0$, for (f) different charge densities σ and (g) radius of nanopores r_0.

instability. The deviation from the linear law becomes weaker as the surface charge density is increased, as shown by the green data in Fig. 3(f). As an example, for a larger surface charge density of $\sigma = 3.121\ e/nm^2$, a direct linear correlation between $\bar{v}$ and $\bar{E}$ is observed. In short, the steeper slope observed in the linear range indicates a higher σ. This elevated σ also results in a reduced probability of encountering a retarded EOF at higher applied voltages (electric fields), indicating a strong resistance to applied electric fields.

Expanding on the previous discussion, we consider the influences of the ion concentration in the bulk solution (c_{bulk}) and the nanopore's radius r_0 on velocity (Fig. S4). The representative relationship between $\bar{v}$ and $\bar{E}$ with various values of r_0 is shown in Fig. 3(g). Since the charge density of the nanopore has been fixed, we find that the slopes of $\bar{v}$ and $\bar{E}$ do not vary much in the linear region. However, the system with a large radius ($r_0 = 4$ nm) shows non-monotonicity earlier with increasing $\bar{E}$, which exhibits a weaker resistance to applied electric fields. For the scenario that the ion concentration ($c_{bulk} = 1$ M) or the radius ($r_0 = 4$ nm) is large, the radial distributions of $\boldsymbol{v}$ at $z = 0$ also show a "W" shape. The reason is that the net charge is 0 near the center ($r = 0$ nm) as shown in [Figs. S4(b) and S4(e)]. Although there is no reverse net charge, it does not cause reverse flow. The physical significance of this is that when the net charge becomes 0, the local driving force becomes 0 and it causes a localized weakening of the velocity. We should note that in the real situation the surface charge cannot be perfectly uniformly distributed, which can affect the property of EOF.

IV. PROTEIN NANOPORES

Unlike solid-state nanopores, protein nanopores possess complicated structures and nonuniform space charge distribution. These characteristics play a key role in the complicated nature of EOF within protein nanopores. In this section, we aim to generalize the EOF properties of three protein nanopores (wild-type), α-HL,

MspA, and CsgG, by applying the results of cylindrical nanopores. Moreover, taking MspA as an example, we discuss the influence of the mutation on EOF.

Given the experimental conditions, our discussion is focused on the results of the following conditions: The applied voltage is 0.12 V and the salt concentration in bulk solution is 1 M. The velocity distributions in two dimensions for α-HL, MspA, and CsgG are presented in Figs. 4(a), 4(d), and 4(g), respectively. In these figures, red and blue colors correspond to positive and negative fluid flows within the protein nanopores. The velocities of EOF $\boldsymbol{v}$ inside all three nanopores exhibit nonhomogeneous distributions. For α-HL, a slightly uneven flow, characterized by regions of heightened flow intensity [Fig. 4(a)], is seen. MspA displays a more concentrated flow, particularly at the constriction point (id: D91) as shown in Fig. 4(d), while CsgG exhibits a mixed flow pattern, including localized reverse flow near the *cis* entrance. Comparing the results for the cylinder in Sec. III, in general, we find that α-HL and MspA have a positive direction of $\boldsymbol{v}$. The behavior of their fluids is closer to the negatively charged cylindrical nanopores. It implies that they prevent the capture of the object from being translocated. Whereas, the $\boldsymbol{v}$ direction in CsgG is negative and therefore closer to a positively charged cylindrical nanopore. Interestingly, the "apparent charges"

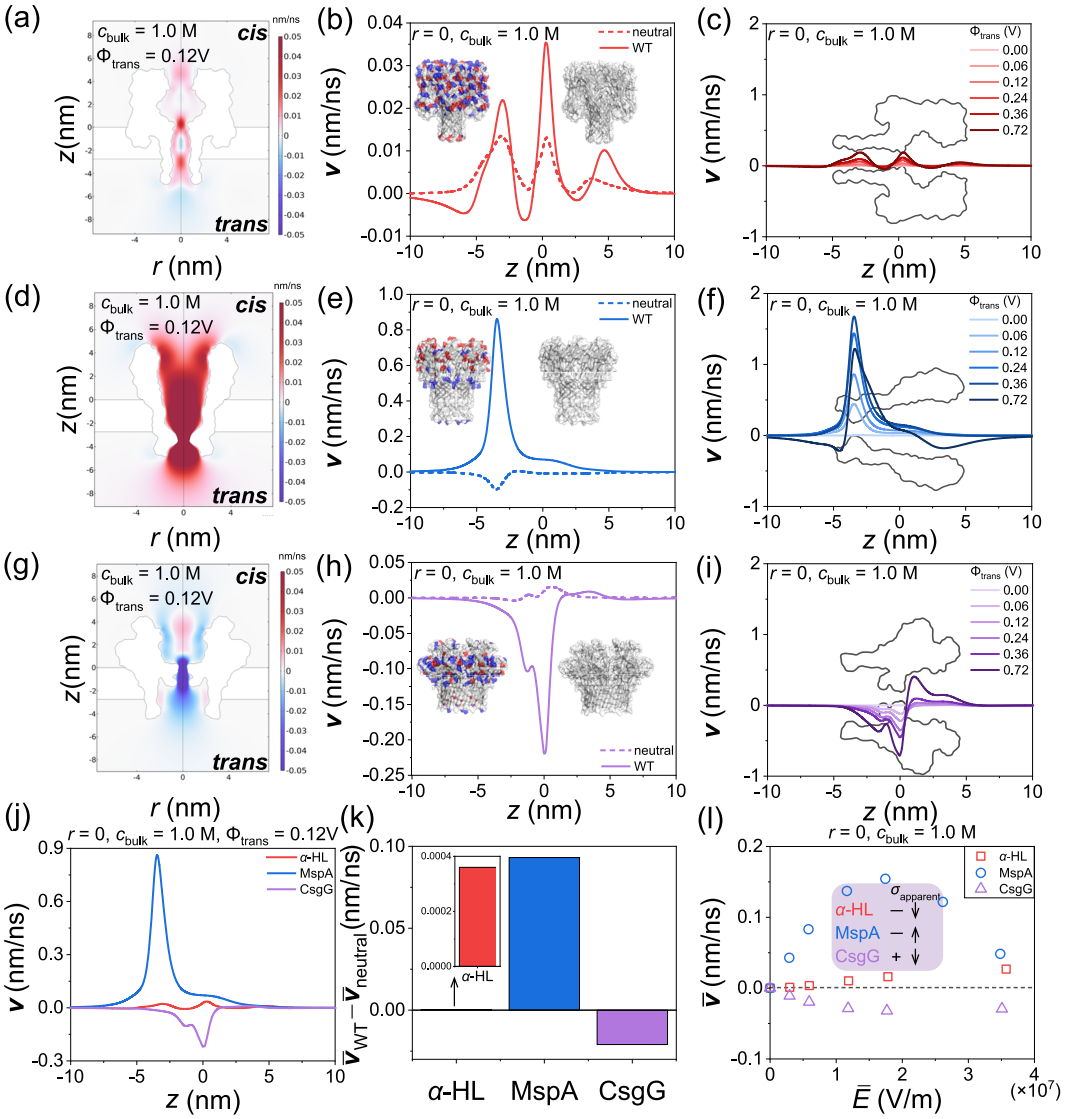

FIG. 4. Velocities of EOF in *r*-*z* plane, comparison of velocities in wild-type (WT) and charge neutral proteins, and velocities in protein nanopores under different applied voltages for (a)–(c) α-HL, (d)–(f) MspA, and (g)–(i) CsgG. (j) Comparison of velocities in the three protein nanopores, $\boldsymbol{v}$ at $r = 0$. (k) Change of the averaged velocities between WT $\bar{v}_{WT}$ and neutral proteins $\bar{v}_{neutral}$. (l) Relationship between velocity $\bar{v}$ and electric field $\bar{E}$ averaged over the vertical direction at $r = 0$, $\sigma_{apparent}$ refers to the "apparent charge density" of protein nanopores.

of these proteins, as inferred from the fluid direction, neither align with their net charges (α-HL: +7 e; MspA: −88 e; CsgG: −9 e) nor the surface charge of the whole protein geometry (α-HL: +9.53 e; MspA: −14.01 e; CsgG: −6.98 e). However, the net charge of the inner surface is −0.33, −2.05, and +1.76 e, respectively, for α-HL, MspA, and CsgG, which is consistent with the "apparent charges." A comparison of $\boldsymbol{v}$ of the three protein nanopores at the longitudinal direction (r = 0 nm) is shown in Fig. 4(j), and all of them have a peak flow velocity at the constriction position, e.g., α-HL at z = 0.29 nm (id: M113), MspA at z = −3.58 nm (id: D91), CsgG at z = 0.23 nm (id: N55 and F56), where the gradients of the electric field and ion concentration are large. The averaged relationship of $\boldsymbol{v}$ among the three nanopores is $\bar{v}_{\mathrm{MspA}} > \bar{v}_{\mathrm{CsgG}} > \bar{v}_{\alpha-\mathrm{HL}}$.

To further explore the effect of charge in the protein nanopore on EOF, we compared $\boldsymbol{v}$ of natural (wild-type, denoted as "WT") and uncharged protein nanopores (only has a geometric shape, denoted as "neutral") in Figs. 4(b), 4(e), 4(h), and 4(k). The results in Fig. 4(b) show that the values of $\boldsymbol{v}$ in both the WT and neutral α-HL are predominantly positive within the nanopore, with minimal variation between them. The results of $\boldsymbol{v}$ in MspA [Fig. 4(e)] display a significant positive velocity peak for the WT condition, but the neutral condition has reduced the velocity. On the other hand, EOF in CsgG demonstrates a prominent negative velocity peak for the WT condition [Fig. 4(h)]. A summary of the change in averaged velocities ($\Delta\bar{v} = \bar{v}_{\mathrm{WT}} - \bar{v}_{\mathrm{neutral}}$) of the three protein pores is illustrated in Fig. 4(k) and Figs. S5(a) and S5(b). The values of $\Delta\bar{v}$ follow the relationship MspA > CsgG > α-HL. We also analyzed the change ratio of the averaged velocities through $\frac{\bar{v}_{\mathrm{WT}} - \bar{v}_{\mathrm{neutral}}}{\bar{v}_{\mathrm{WT}}}$ (Fig. S5a). For MspA and CsgG, the ratios are close, and both of them are larger than 1, which means that the velocities have reversed. The change ratio for α-HL is only 0.1, and there is no velocity reversal.

A comparison of EOF of three nanopores under different applied voltages is shown in Figs. 4(c), 4(f), and 4(i). In this analysis, the velocities within the three protein nanopores exhibit fluctuations at the constriction region with increasing applied voltage. However, these localized fluctuations result in a more substantial velocity of the opposing flow, consequently diminishing the average EOF velocity $\boldsymbol{v}$. The summarized results of the relationship between $\bar{\boldsymbol{v}}$ and $\bar{E}$ are shown in Fig. 4(l). Both MspA and CsgG exhibit a nonlinear relationship, but in the linear regions, MspA has a much steeper slope than CsgG. According to the conclusions drawn in the cylindrical nanopores [Figs. 3(d) and 3(e)], MspA exhibits a larger surface charge density. MspA and CsgG, respectively, have the negative and positive "apparent charge." In the weak electric fields, the velocity is proportional to the applied electric field as mentioned in the discussion of solid-state nanopore. However, as the applied electric field becomes stronger, the above-mentioned local velocity reversal becomes significant, resulting in a retardation effect on the net EOF velocity. The direct reason is the reversal of the local net charge. Taking CsgG as an example (Fig. S5e), with the increasing of the electric fields, the local net charge changing from negative to 0 or larger than 0 M. Interestingly, the relationship between $\bar{\boldsymbol{v}}$ and $\bar{E}$ for α-HL shows a linear trend with a weaker slope, which means that α-HL has a strong resistance to the applied electric field even though with a low charge density. This resistance can be attributed to its smaller nanopore radius region, from the constriction position (z = 0.29 nm, id: M113) to the *trans* side, where the electrostatic effects from the amino acids play a significant role.

The engineering of protein nanopores has been the focus of research in the field of translocation. The more mature is the modification of MspA, compared to WT currently more commonly used in experiments are M1-MspA and M2-MspA. In order to investigate the impact of these mutations on the EOF, we have chosen to use MspA as a representative example, as illustrated in Fig. 5. The mutation points of M1-MspA and M2-MspA present schematically in Fig. 5(a). The only deviation in the calculation procedure compared to WT-MspA involved the utilization of the CHARMM-GUI tool to introduce mutations based on the PDB file of WT-MspA.[40] These mutations have reduced the negative charge carried by MspA; specifically, M1-MspA carries −64 e and M2-MspA carries −16 e charges. Although the mutation only changes 3 (M1-MspA) or 6 (M2-MspA) sites on each monomer, this directly resulted in a reversal of the average EOF direction [Figs. 5(b) and 5(c)]. Both the M1-MspA and M2-MspA exhibit a negative direction of EOF, which proves valuable in slowing down the translocation of analytes (such as DNA, RNA, or peptides) during experiments. From the relationship between $\bar{\boldsymbol{v}}$ and $\bar{E}$ in Fig. 5(d), M1-MspA and M2-MspA behave like a positively charged pore with a small charge density. This conclusion aligns with our research findings, and this behavior is likely influenced by the net charge of the inner surface, with M1-MspA having a net charge of +1.82 e and M2-MspA having a net charge of +11.92 e.

To verify the accuracy of our predictions, we made comparisons of our results with experimental or simulation data, our predictions are consistent with the other studies and can further provide explanations for the data. For example, the results of α-HL presented in the work of Asandei *et al.* have shown that the number of electro-osmotic flow is close to zero and has fluctuations of the direction when $\Phi_{trans} > 0$ and pH = 7.[55] From our calculation results [Figs. 4(a)–4(c)], the velocity is also small and close to zero, and the fluctuations of the direction may come from the localized reversal of water molecule flow. The velocity of EOF in CsgG according to Chinappi's group shows that $\boldsymbol{v} \approx -0.26$ nm/ns at the applied voltage $\Phi_{trans} \approx 0.11$ V.[23] This number is in the same magnitude of our numerical prediction in Fig. 4(h).

In summary, the data provide valuable insights into the complexities of EOF in protein nanopores. Each of the three nanopores, α-HL, MspA, and CsgG, exhibits unique EOF profiles. Judging from these velocity properties, we can draw the following conclusions. In general, α-HL behaves like a negatively charged pore with a smaller charge density and higher voltage resistance; WT-MspA behaves like a negatively charged pore with a larger charge density and lower voltage resistance; CsgG behaves like a positively charged pore with a smaller charge density and lower voltage resistance. Some effective point mutations can significantly change the EOF properties, e.g., M1-MspA and M2-MspA can directly lead to the reversal of EOF, making MspA behave from a strongly negatively charged property (WT) to weak positively charged (M1 and M2). In practical applications, increasing the applied voltage does not necessarily guarantee an improvement in EOF velocity and may even lead to increased internal fluid instability, which is detrimental to sequencing accuracy.

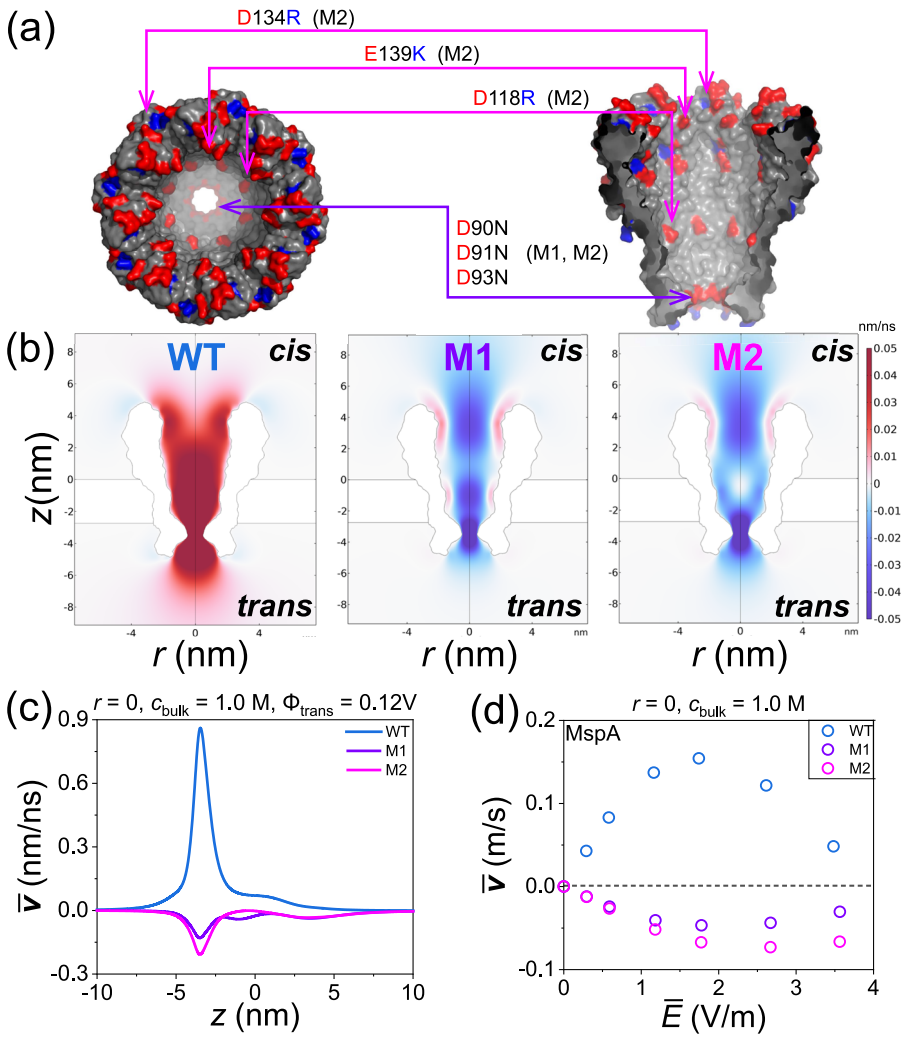

FIG. 5. Comparison of velocities in wild-type and point mutations of MspA. (a) Structure and charge distribution of wild-type MspA, the cartoon is generated by PyMOL.[54] Aspartate and glutamate residues are colored red (negatively charged), and arginine and lysine residues (positively charged) are colored blue. Locations and identities of mutations are indicated by arrows and labels: mutant of M1-MspA, D90N/D91N/D93N; mutant of M2-MspA, D90N/D91N/D93N/D118R/E139K/D134R. (b), (c) Comparison of velocities $\boldsymbol{v}$ in r-z plane and at $r = 0$, where $\Phi_{trans} = 0.12$ V and $c_{bulk} = 1$ M. (d) Relationship between velocity $\bar{v}$ and electric field $\bar{E}$ averaged over the vertical direction at $r = 0$.

V. CONCLUSIONS

The geometry and charges of nanopores have a profound impact on the signal response during sequencing, and substantial progress has been made in designing nanopores to enhance sequencing accuracy, including solid-state nanopores and engineered protein nanopores. These nanopores create particular EOFs, and understanding EOF is crucial for improving the accuracy of nanopore sequencing devices. Protein nanopores, characterized by their complex geometries and variable charge distributions, present unique challenges for studying EOF. In this work, we propose an idea of applying EOF properties in classical models, i.e. cylindrical geometry, to comparatively study EOF in complex protein nanopores.

By systematically examining the following factors of the cylindrical nanopore, namely, charge density of the nanopore's inner surface, applied voltage, ion concentration in the bulk solution, and the nanopore's radius, we find that the effects of these factors on EOF essentially stem from competition between the forces from the charged interface and the longitudinal electric field. When the nanopore surface strongly attracts counterions, a more robust EOF velocity is produced, and it offers greater resistance to the external electric field. The mean velocity exhibits a direct relationship with the electric field's intensity. Conversely, if this attraction is weak, the flow velocity diminishes, and there's a pattern where the average velocity first increases with the electric field and then decreases as the electric field intensifies. Positively charged

nanopores induce EOF opposing the electric field direction, whereas negatively charged ones produce EOF that complements the electric field, and we have quantified these effects by numerically solving the coupled Poisson–Nernst–Planck formalism and the Navier–Stokes equation.

We have further explored the velocities of EOF in three commonly used protein nanopores: α-HL, MspA, and CsgG. Extending our findings from the cylindrical nanopore, we present details of the EOF characteristics of these three protein nanopores through the "apparent charge density." (a) α-HL is characterized by a nanopore with negative charge, albeit with a lower charge density, and it exhibits greater resistance to voltage. (b) WT-MspA exhibits negative charge, but with a higher charge density, and it displays lower resistance to voltage. Mutations of WT-MspA, M1-MspA, and M2-MspA show a weak positive charge density with stronger resistance to voltage than WT-MspA. This study provides insight into the intricate behavior of EOF within nanoconfinement, with a particular focus on the influences of the charge pattern and geometry of the nanopores. The method and findings proposed here can serve as a potential guide for designing future nanopore systems and hold promise for enhancing the accuracy and efficiency of nanopore-based sequencing technologies.

SUPPLEMENTARY MATERIAL

The supplementary material contains the additional figures.

ACKNOWLEDGMENTS

The authors thank the National Science Foundation (Grant No. DMR 2309539) and AFOSR (Grant No. FA9550-23-1-0584). The authors also thank Dr. Kaikai Zheng (Center for Soft and Living Matter, Institute for Basic Science, Korea) for support of computer software.

AUTHOR DECLARATIONS

Conflict of Interest

The authors have no conflicts to disclose.

Author Contributions

Minglun Li: Conceptualization (equal); Data curation (equal); Formal analysis (equal); Writing – original draft (equal); Writing – review & editing (equal). **Murugappan Muthukumar**: Conceptualization (lead); Project administration (lead); Supervision (lead); Writing – review & editing (equal).

DATA AVAILABILITY

The data that support the findings of this study are available within the article.

REFERENCES

[1]D. Branton, D. W. Deamer, A. Marziali, H. Bayley, S. A. Benner, T. Butler, M. Di Ventra, S. Garaj, A. Hibbs, X. Huang *et al.*, "The potential and challenges of nanopore sequencing," Nat. Biotechnol. **26**, 1146–1153 (2008).
[2]D. Deamer, M. Akeson, and D. Branton, "Three decades of nanopore sequencing," Nat. Biotechnol. **34**, 518–524 (2016).
[3]H. Brinkerhoff, A. S. Kang, J. Liu, A. Aksimentiev, and C. Dekker, "Multiple rereads of single proteins at single–amino acid resolution using nanopores," Science **374**, 1509–1513 (2021).
[4]M. Afshar Bakshloo, J. J. Kasianowicz, M. Pastoriza-Gallego, J. Mathé, R. Daniel, F. Piguet, and A. Oukhaled, "Nanopore-based protein identification," J. Am. Chem. Soc. **144**, 2716–2725 (2022).
[5]J. Bai, D. Wang, S.-w. Nam, H. Peng, R. Bruce, L. Gignac, M. Brink, E. Kratschmer, S. Rossnagel, P. Waggoner *et al.*, "Fabrication of sub-20 nm nanopore arrays in membranes with embedded metal electrodes at wafer scales," Nanoscale **6**, 8900–8906 (2014).
[6]Y. Yao, C. Wen, N. H. Pham, and S.-L. Zhang, "On induced surface charge in solid-state nanopores," Langmuir **36**, 8874–8882 (2020).
[7]K. Chen and M. Muthukumar, "Substantial slowing of electrophoretic translocation of DNA through a nanopore using coherent multiple entropic traps," ACS Nano **17**, 9197–9208 (2023).
[8]Y. Qing, S. A. Ionescu, G. S. Pulcu, and H. Bayley, "Directional control of a processive molecular hopper," Science **361**, 908–912 (2018).
[9]M. Muthukumar, *Polymer Translocation* (CRC Press, 2016).
[10]R. B. Schasfoort, S. Schlautmann, J. Hendrikse, and A. Van Den Berg, "Field-effect flow control for microfabricated fluidic networks," Science **286**, 942–945 (1999).
[11]M. Mirzadeh, T. Zhou, M. A. Amooie, D. Fraggedakis, T. R. Ferguson, and M. Z. Bazant, "Vortices of electro-osmotic flow in heterogeneous porous media," Phys. Rev. Fluids **5**, 103701 (2020).
[12]A. Gupta, P. J. Zuk, and H. A. Stone, "Charging dynamics of overlapping double layers in a cylindrical nanopore," Phys. Rev. Lett. **125**, 076001 (2020).
[13]Q. Pan, X. Lin, S. Wei, J. Su, H. Zhao, X. Duan, G. Hu, and Y. He, "Spatiotemporally controlled emergence of nanoparticle microvortices under electric field," Aggregate (published online).
[14]S. Van Dorp, U. F. Keyser, N. H. Dekker, C. Dekker, and S. G. Lemay, "Origin of the electrophoretic force on DNA in solid-state nanopores," Nat. Phys. **5**, 347–351 (2009).
[15]S. Nam, I. Cho, J. Heo, G. Lim, M. Z. Bazant, D. J. Moon, G. Y. Sung, and S. J. Kim, "Experimental verification of overlimiting current by surface conduction and electro-osmotic flow in microchannels," Phys. Rev. Lett. **114**, 114501 (2015).
[16]X. Shi, A.-K. Pumm, J. Isensee, W. Zhao, D. Verschueren, A. Martin-Gonzalez, R. Golestanian, H. Dietz, and C. Dekker, "Sustained unidirectional rotation of a self-organized DNA rotor on a nanopore," Nat. Phys. **18**, 1105–1111 (2022).
[17]U. F. Keyser, B. N. Koeleman, S. Van Dorp, D. Krapf, R. M. Smeets, S. G. Lemay, N. H. Dekker, and C. Dekker, "Direct force measurements on DNA in a solid-state nanopore," Nat. Phys. **2**, 473–477 (2006).
[18]S. Schmid, P. Stömmer, H. Dietz, and C. Dekker, "Nanopore electro-osmotic trap for the label-free study of single proteins and their conformations," Nat. Nanotechnol. **16**, 1244–1250 (2021).
[19]G. Huang, K. Willems, M. Bartelds, P. Van Dorpe, M. Soskine, and G. Maglia, "Electro-osmotic vortices promote the capture of folded proteins by PlyAB nanopores," Nano Lett. **20**, 3819–3827 (2020).
[20]C. T. A. Wong and M. Muthukumar, "Polymer capture by electro-osmotic flow of oppositely charged nanopores," J. Chem. Phys. **126**, 164903 (2007).
[21]M. Muthukumar, "Theory of capture rate in polymer translocation," J. Chem. Phys. **132**, 195101 (2010).
[22]S. Ghosal, "Effect of salt concentration on the electrophoretic speed of a polyelectrolyte through a nanopore," Phys. Rev. Lett. **98**, 238104 (2007).
[23]G. Di Muccio, B. Morozzo della Rocca, and M. Chinappi, "Geometrically induced selectivity and unidirectional electroosmosis in uncharged nanopores," ACS Nano **16**, 8716–8728 (2022).

[24]J. Yoo and A. Aksimentiev, "Molecular dynamics of membrane-spanning DNA channels: Conductance mechanism, electro-osmotic transport, and mechanical gating," J. Phys. Chem. Lett. **6**, 4680–4687 (2015).
[25]E. L. Bonome, F. Cecconi, and M. Chinappi, "Electroosmotic flow through an α-hemolysin nanopore," Microfluid. Nanofluid. **21**, 96 (2017).
[26]L. Song, M. R. Hobaugh, C. Shustak, S. Cheley, H. Bayley, and J. E. Gouaux, "Structure of staphylococcal α-hemolysin, a heptameric transmembrane pore," Science **274**, 1859–1865 (1996).
[27]M. Faller, M. Niederweis, and G. E. Schulz, "The structure of a mycobacterial outer-membrane channel," Science **303**, 1189–1192 (2004).
[28]P. Goyal, P. V. Krasteva, N. Van Gerven, F. Gubellini, I. Van den Broeck, A. Troupiotis-Tsaïlaki, W. Jonckheere, G. Péhau-Arnaudet, J. S. Pinkner, M. R. Chapman *et al.*, "Structural and mechanistic insights into the bacterial amyloid secretion channel CsgG," Nature **516**, 250–253 (2014).
[29]Y. Liu, K. Wang, Y. Wang, L. Wang, S. Yan, X. Du, P. Zhang, H.-Y. Chen, and S. Huang, "Machine learning assisted simultaneous structural profiling of differently charged proteins in a *Mycobacterium smegmatis* porin A (MspA) electroosmotic trap," J. Am. Chem. Soc. **144**, 757–768 (2022).
[30]D. Jones, J. E. Allen, Y. Yang, W. F. Drew Bennett, M. Gokhale, N. Moshiri, and T. S. Rosing, "Accelerators for classical molecular dynamics simulations of biomolecules," J. Chem. Theory Comput. **18**, 4047–4069 (2022).
[31]K. Willems, D. Ruić, F. L R Lucas, U. Barman, N. Verellen, J. Hofkens, G. Maglia, and P. Van Dorpe, "Accurate modeling of a biological nanopore with an extended continuum framework," Nanoscale **12**, 16775–16795 (2020).
[32]Y. Qiu and L. Ma, "Influences of electroosmotic flow on ionic current through nanopores: A comprehensive understanding," Phys. Fluids **34**, 112010 (2022).
[33]M. G. Kurnikova, R. D. Coalson, P. Graf, and A. Nitzan, "A lattice relaxation algorithm for three-dimensional Poisson-Nernst-Planck theory with application to ion transport through the gramicidin A channel," Biophys. J. **76**, 642–656 (1999).
[34]B. Roux, "Influence of the membrane potential on the free energy of an intrinsic protein," Biophys. J. **73**, 2980–2989 (1997).
[35]W. Im and B. Roux, "Brownian dynamics simulations of ions channels: A general treatment of electrostatic reaction fields for molecular pores of arbitrary geometry," J. Chem. Phys. **115**, 4850–4861 (2001).
[36]W. Im and B. Roux, "Ion permeation and selectivity of OmpF porin: A theoretical study based on molecular dynamics, Brownian dynamics, and continuum electrodiffusion theory," J. Mol. Biol. **322**, 851–869 (2002).
[37]I. Jou and M. Muthukumar, "Effects of nanopore charge decorations on the translocation dynamics of DNA," Biophys. J. **113**, 1664–1672 (2017).
[38]L. D. Landau and E. M. Lifshitz, *Fluid Mechanics: Landau and Lifshitz: Course of Theoretical Physics* (Elsevier, 2013), Vol. 6.
[39]E. D. Pederson, J. Barbalas, B. S. Drown, M. J. Culbertson, L. M. Keranen Burden, J. J. Kasianowicz, and D. L. Burden, "Proximal capture dynamics for a single biological nanopore sensor," J. Phys. Chem. B **119**, 10448–10455 (2015).
[40]S. Jo, T. Kim, V. G. Iyer, and W. Im, "CHARMM-GUI: A web-based graphical user interface for CHARMM," J. Comput. Chem. **29**, 1859–1865 (2008).
[41]H. M. Berman, J. Westbrook, Z. Feng, G. Gilliland, T. N. Bhat, H. Weissig, I. N. Shindyalov, and P. E. Bourne, "The protein data bank," Nucleic Acids Res. **28**, 235–242 (2000).
[42]E. Jurrus, D. Engel, K. Star, K. Monson, J. Brandi, L. E. Felberg, D. H. Brookes, L. Wilson, J. Chen, K. Liles *et al.*, "Improvements to the APBS biomolecular solvation software suite," Protein Sci. **27**, 112–128 (2018).
[43]APBS-PDB2PQR: https://server.poissonboltzmann.org/ (2023).
[44]M. H. Olsson, C. R. Søndergaard, M. Rostkowski, and J. H. Jensen, "PROPKA3: Consistent treatment of internal and surface residues in empirical pK_a predictions," J. Chem. Theory Comput. **7**, 525–537 (2011).
[45]C. R. Søndergaard, M. H. Olsson, M. Rostkowski, and J. H. Jensen, "Improved treatment of ligands and coupling effects in empirical calculation and rationalization of pK_a values," J. Chem. Theory Comput. **7**, 2284–2295 (2011).
[46]L. Li, C. Li, Z. Zhang, and E. Alexov, "On the dielectric "constant" of proteins: Smooth dielectric function for macromolecular modeling and its implementation in DelPhi," J. Chem. Theory Comput. **9**, 2126–2136 (2013).
[47]B. R. Brooks, C. L. Brooks III, A. D. Mackerell, Jr., L. Nilsson, R. J. Petrella, B. Roux, Y. Won, G. Archontis, C. Bartels, S. Boresch *et al.*, "CHARMM: The biomolecular simulation program," J. Comput. Chem. **30**, 1545–1614 (2009).
[48]D. A. Case, T. E. Cheatham III, T. Darden, H. Gohlke, R. Luo, K. M. Merz, Jr., A. Onufriev, C. Simmerling, B. Wang, and R. J. Woods, "The Amber biomolecular simulation programs," J. Comput. Chem. **26**, 1668–1688 (2005).
[49]A. Aksimentiev and K. Schulten, "Imaging α-hemolysin with molecular dynamics: Ionic conductance, osmotic permeability, and the electrostatic potential map," Biophys. J. **88**, 3745–3761 (2005).
[50]J. P. Fried, J. L. Swett, B. P. Nadappuram, J. A. Mol, J. B. Edel, A. P. Ivanov, and J. R. Yates, "*In situ* solid-state nanopore fabrication," Chem. Soc. Rev. **50**, 4974–4992 (2021).
[51]J. N. Israelachvili, *Intermolecular and Surface Forces* (Academic Press, 2011).
[52]M. Z. Bazant, B. D. Storey, and A. A. Kornyshev, "Double layer in ionic liquids: Overscreening versus crowding," Phys. Rev. Lett. **106**, 046102 (2011).
[53]A. Gupta, A. Govind Rajan, E. A. Carter, and H. A. Stone, "Ionic layering and overcharging in electrical double layers in a Poisson-Boltzmann model," Phys. Rev. Lett. **125**, 188004 (2020).
[54]Schrödinger, LLC, The PyMOL molecular graphics system, Version 1.8 (2015).
[55]A. Asandei, I. Schiopu, M. Chinappi, C. H. Seo, Y. Park, and T. Luchian, "Electroosmotic trap against the electrophoretic force near a protein nanopore reveals peptide dynamics during capture and translocation," ACS Appl. Mater. Interfaces **8**, 13166–13179 (2016).